Supporting information:

$SrTiO_3/Bi_4Ti_3O_{12}$ Nanoheterostructural Platelets Synthesized by Topotactic Epitaxy as Effective Noble-Metal-Free Photocatalysts for pH-Neutral Hydrogen Evolution

Marjeta Maček Kržmanc*† Nina Daneu†, Alja Čontala†‡, Saswati Santra†, Khaja Mohaideen Kamal #, Blaž Likozar# and Matjaž Spreitzer†

† Advanced Materials Department, Jožef Stefan Institute, Jamova cesta 39, 1000 Ljubljana, Slovenia

‡ Jožef Stefan International Postgraduate School, Jamova cesta 39, 1000 Ljubljana, Slovenia

Department of Catalysis and Chemical Reaction Engineering, National Institute of Chemistry, Hajdrihova 19, 1000 Ljubljana, Slovenia

Corresponding author:
Marjeta Maček Kržmanc: marjeta.macek@ijs.si

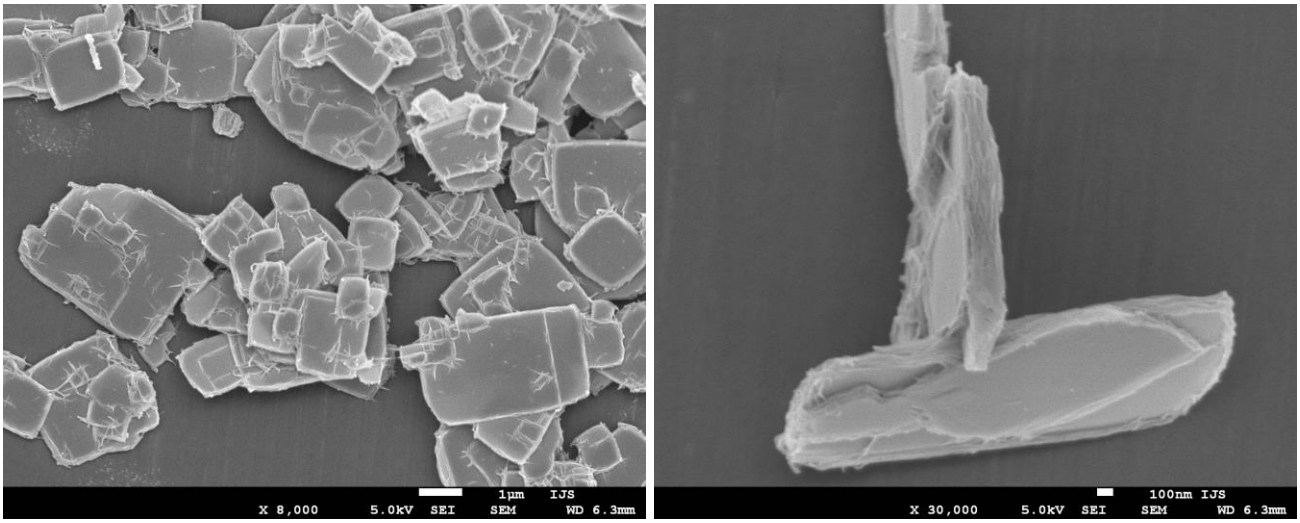

Figure S1: SEM micrographs of the $Bi_4Ti_3O_{12}$ platelets after treatment in 6-M NaOH (in the absence of Sr^{2+} ions) at 200°C for 15 hours.

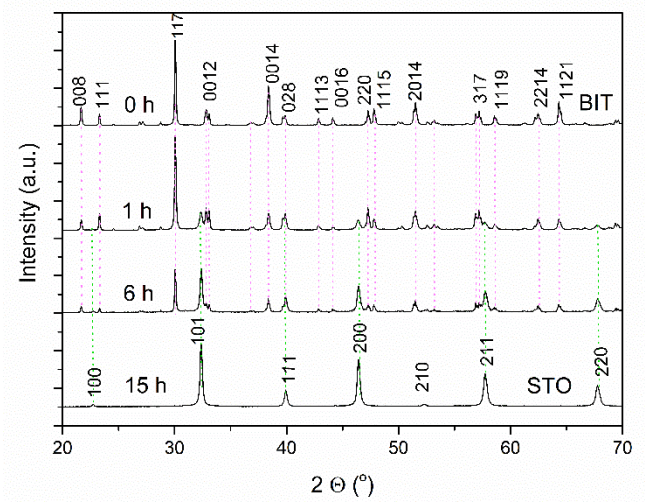

Figure S2: Powder XRD patterns of the of the HNO_3-washed platelets after different times of TC reaction (200°C, 6-M NaOH, Sr/Ti=12). The STO and BIT abbreviations stand for $SrTiO_3$ and $Bi_4Ti_3O_{12}$, respectively.

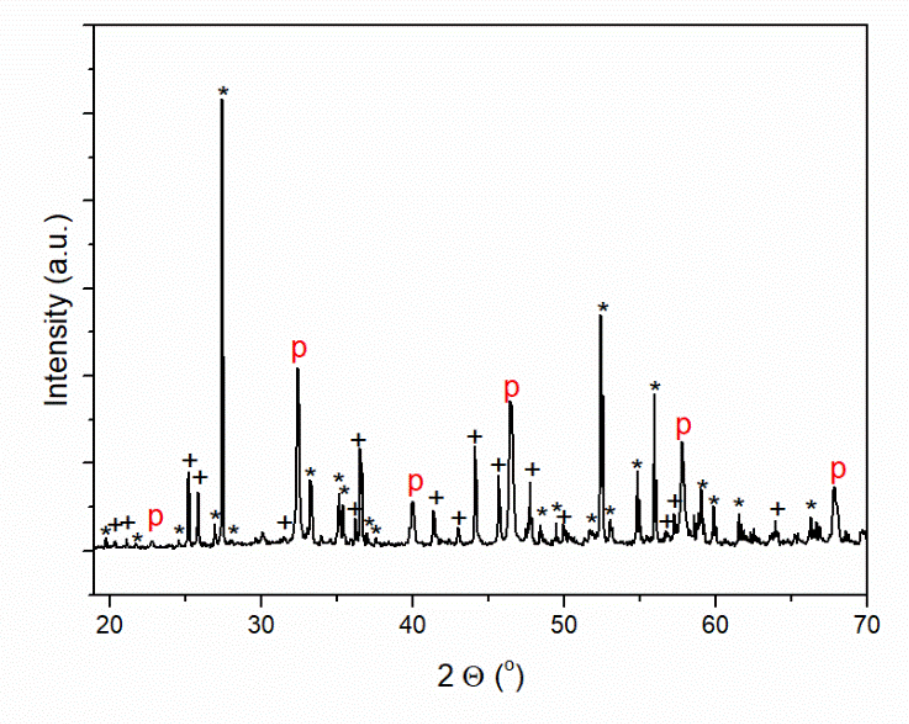

Figure S3: XRD pattern of the water-washed reaction product, obtained at Sr/Ti=12, 200°C/15 hours, 6-M NaOH: p⇒$SrTiO_3$ perovskite, *⇒Bi_2O_3, +⇒$SrCO_3$.

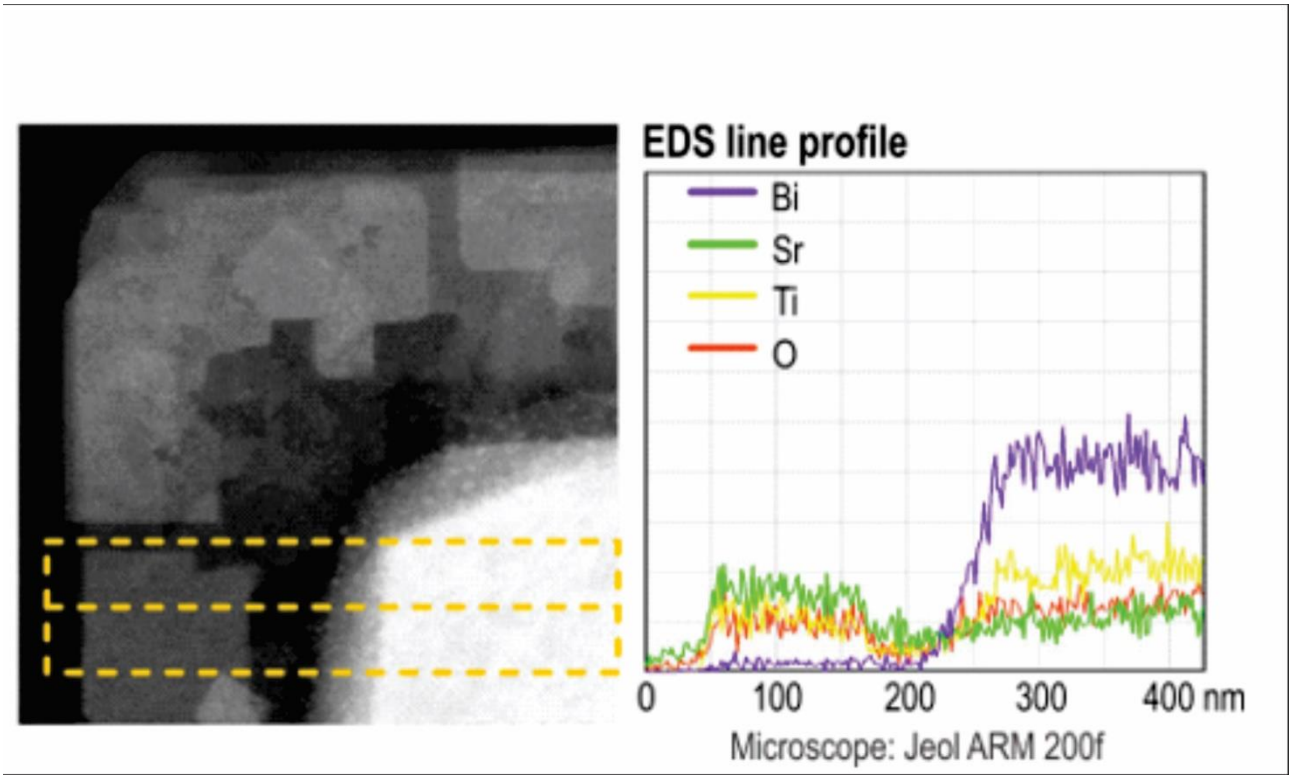

Figure S4: STEM (DF with EDS line profile) of $SrTiO_3/Bi_4Ti_3O_{12}$ heterostructural platelet formed after 1 hour at 200°C at Sr/Ti=12 and 6-M NaOH.

Theoretical calculation of platelet-thickness difference during transformation of pre-existing $Bi_4Ti_3O_{12}$ (BIT) platelets to $SrTiO_3$ (STO) platelets, assuming a constant length and width of the platelets:

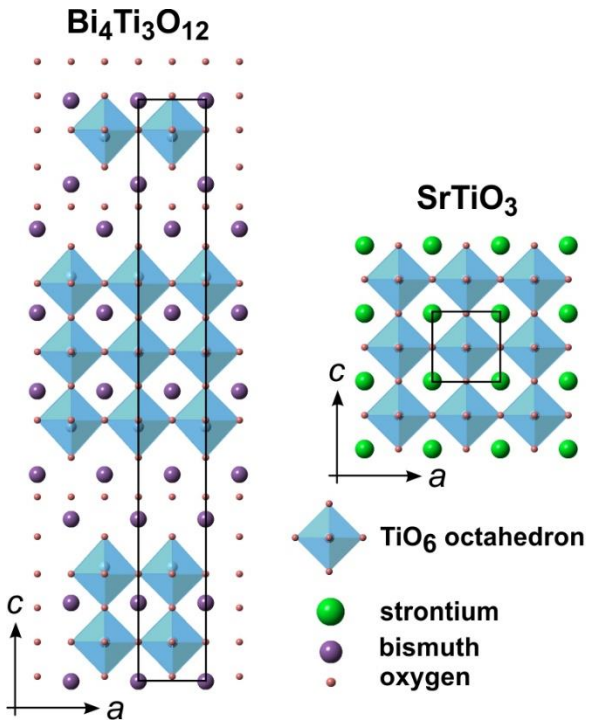

Figure S5: Structural models of $Bi_4Ti_3O_{12}$ and $SrTiO_3$

c_{BIT} = 3.2882 nm

c_{STO} = 0.3905 nm

One BIT unit cell contains 6 TiO_6 octahedra along the c-direction. Theoretically, these convert to TiO_6 octahedra in the newly formed STO, where the unit cell extends across one TiO_6 octahedron.

1 $c_{BIT} \rightarrow$ 6 c_{STO}

c_{BIT} = 3.2882 nm

c_{STO} = 0.3905 nm; **6·c_{STO} = 2.343 nm**

(6·c_{STO} / c_{BIT})·100 = 71.25 %

The calculation indicates that a BIT platelet with an average thickness of ~ 60 nm would transform into an STO platelet with a thickness of ~ 42 nm.

Table S1: H_2-evolution rates ($\mu mol\ g^{-1} \cdot h^{-1}$) of $Bi_4Ti_3O_{12}$, $SrTiO_3/Bi_4Ti_3O_{12}$ and $SrTiO_3$ platelets and commercial $SrTiO_3$ nanopowders (Figure 6)

Photocatalysts (synthesis time)	Composition-structure	Rate of H_2 evolution ($\mu mol\ g^{-1} \cdot h^{-1}$)	BET ($m^2 g^{-1}$)
$Bi_4Ti_3O_{12}$ platelets (0 hour)	$Bi_4Ti_3O_{12}$	7.5	2–3
$SrTiO_3/Bi_4Ti_3O_{12}$ platelets (6 hours)	$SrTiO_3$: $Bi_4Ti_3O_{12}$=60:40	1265	20
$SrTiO_3$ platelets (15 hours)	$SrTiO_3$	65	10
$SrTiO_3$ commercial nanopowder	$SrTiO_3$	81	24

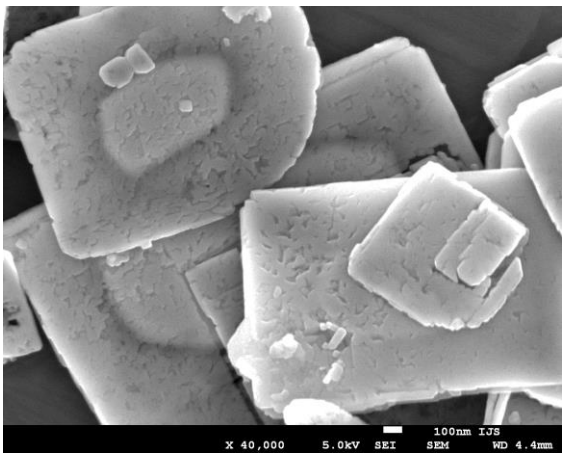

Figure S6: SEM micrograph of the $SrTiO_3/Bi_4Ti_3O_{12}$ nanoheterostructural platelets obtained after 6 hours of reaction at 200°C (Sr/Ti=12, 6-M NaOH).

Table S2: Literature review of various photocatalysts, their H_2-evolution rates and photocatalytic performance evaluation conditions

Photocatalyst	H_2 evolution in μmol $g^{-1}{\cdot}h^{-1}$ (STH)[a]	Irradiation source	Sacrificial agent	Reference
$SrTiO_3/Bi_4Ti_3O_{12}$ nanoheterostructural platelets	**1265 (0.19 %)**	**300-W Xenon lamp with AM 1.5G**	**methanol**	**This work**
$Rh_{2-y}Cr_yO_3$/Al:$SrTiO_3$	530	150-W Xenon lamp with Oriel Cornerstone 130 monochromator filter	Not used	[1]
Pt/ Single-Crystal-Like Porous $SrTiO_3$ Nanocube Assemblies	202.6	300-W Xenon lamp	methanol	[2]
Pt/ mesoporous-assembled $SrTiO_3$ nanocrystal	188	300-W Xenon lamp with UV cut-off filter (>400 nm)	methanol	[3]
N-TiO2/Pt	570	500-W Xe lamp	methanol	[4]
H_2PtCl_6/Copper–Organic Framework	32	200-W Xe lamp (wavelength: 320-780 nm)	methanol	[5]
Pt–Co/g-C_3N_4	61	300-W Xeon lamp (wavelength> 300 nm)	Not used	[6]
Rh/La:$SrTiO_3$	280 (0.037 %)	300-W Xe lamp with cut-off filter (wavelength> 420 nm)	methanol	[7]

[a]*For other cases the STH efficiencies were not reported*

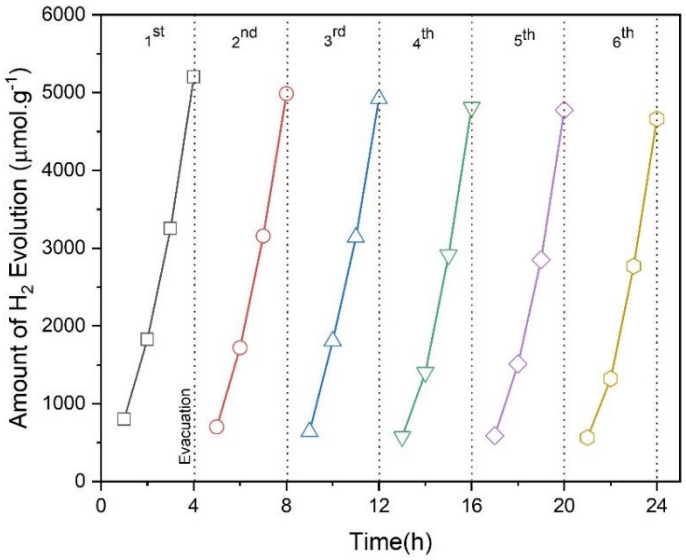

Figure S7: Stability test of H_2 evolution for $SrTiO_3/Bi_4Ti_3O_{12}$ nanoheterostructural platelets obtained after 6-hour hydrothermal reaction ($SrTiO_3$: $Bi_4Ti_3O_{12}$=60:40). After every 4 h of reaction, the formed H_2 was evacuated.

Calculation of the band-gap energy:

The band-gap energies (Eg) of the constituents were calculated using the well-known Tauc method from the UV-VIS diffuse reflectance spectra and Kubelka-Munk function (F(R)) by means of the following equation:[8]

$$F(R) = \frac{K}{S} = \frac{(1-R)^2}{2R}$$

where K and S are the absorption and scattering coefficients, respectively, and R=Rsample/Rstandard. Combination of F(R) into Tauc method provides: $(F(R) \cdot h\nu)^{1/2}$ =B (hν-E_g)

Here, h is the Planck constant, ν is the incident frequency and B is a constant.[8] Figure S6 shows the $(F(R) \cdot h\nu)^{1/2}$ versus hν plots. The band gaps (E_g) of $SrTiO_3$ and $Bi_4Ti_3O_{12}$, which were determined by extrapolation of the linear part of the function at F(R)=0, are 3.23 eV and 3.16 eV, respectively.

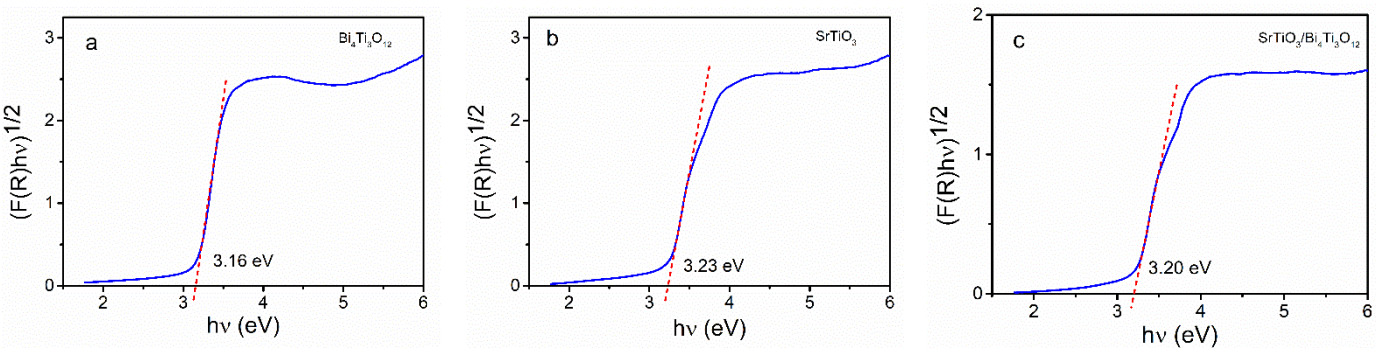

Figure S8: Determination of the band-gap energy from the Tauc plot for (a) $Bi_4Ti_3O_{12}$, (b) $SrTiO_3$ and (c) $SrTiO_3/Bi_4Ti_3O_{12}$ platelets.

Calculation of the position of the conduction band (E_{CB}) and valance band (E_{VB}) energies:

The E_{CB} and E_{VB} are calculated using the following empirical formulas:[9–11]

$$E_{CB} = \chi_{mol} - E_e - 0.5E_g \text{ [1]}$$

$$E_{VB} = E_{CB} + E_g \text{ [2]}$$

Here, Ee is the free-electron energy vs. hydrogen (4.5 eV) and χ_{mol} is the geometric mean of Mulliken's electron negativities of constituent atoms, calculated according to the following equation:[10]

$$\chi_{mol} = [\chi_A^a \cdot \chi_B^b \cdot \chi_C^c]^{\frac{1}{a+b+c}}$$

where the molecular formula is $A_aB_bC_c$. χ_A (χ_B, χ_C) is Mulliken's absolute electronegativity of the corresponding atom (in eV) and it is defined as the arithmetic mean of the electron affinity and the first ionization energy of that atom.[12,13] For $SrTiO_3$ and $Bi_4Ti_3O_{12}$ the calculations give χ_{SrTiO3}=5.32 and $\chi_{Bi4Ti3O12}$=5.87. Considering the calculated values for χ_{SrTiO3} (5,32) and $\chi_{Bi4Ti3O12}$ (5,87), the E_{CB} and E_{VB} of $SrTiO_3$ were determined to be -0.80 eV and 2.43 eV, while for $Bi_4Ti_3O_{12}$ the calculations revealed E_{CB}=-0.21 eV and E_{VB}=2.95 eV, respectively.

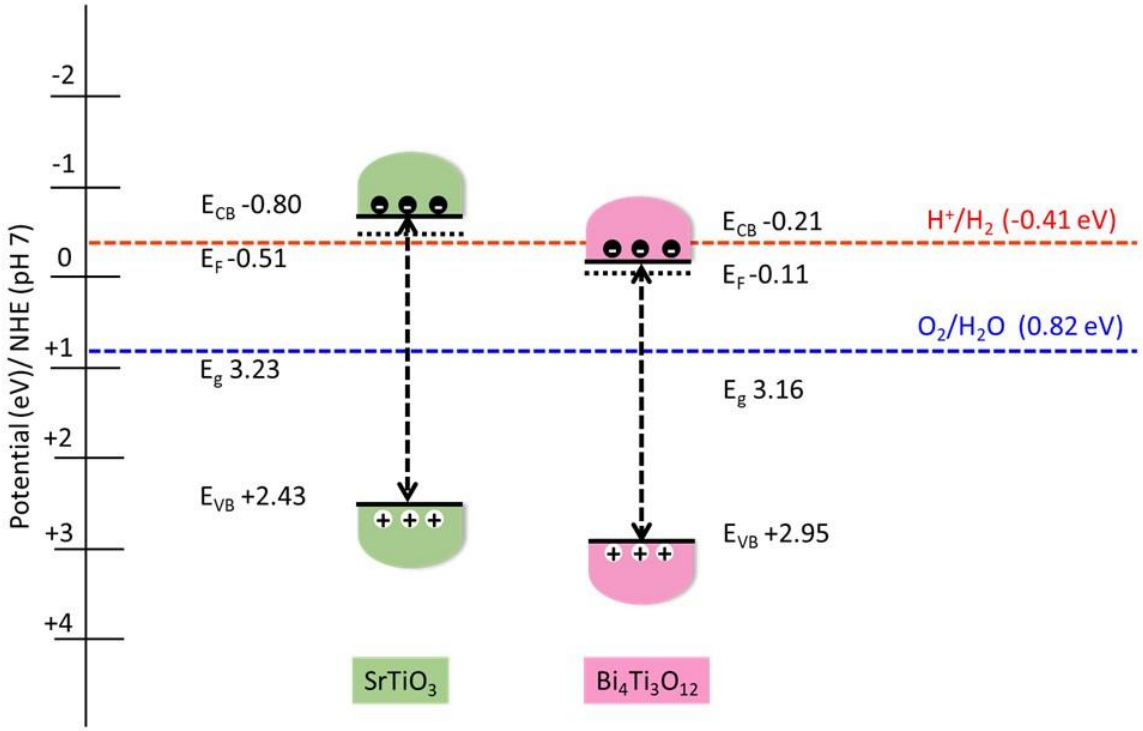

Figure S9: Band structure of $SrTiO_3$ and $Bi_4Ti_3O_{12}$

Calculation of the solar-to-hydrogen (STH) efficiency:

$$STH\ (\%) = \frac{r_{H2} x \Delta G_{H2O}}{P_{Sun} x S} x 100$$

Here, $r_{H2,}$ ΔG_{H2O}, P_{sun} and S represent the H_2 production rate, the reaction Gibbs free energy (237 kJ/mol), the light energy flux ($1.0x10^3$ Wm^{-2}) and irradiation area (9 cm^2), respectively.

Table S3: Comparison of solar-to-hydrogen (STH) efficiencies for $SrTiO_3$-based photocatalytic H_2 evolution

Catalyst	STH (%)	Irradiation source	Reference
Rh/La:$SrTiO_3$	0.037	300-W Xe lamp	[7]
$SrTiO_3$:La, Rh and $BiVO_4$:Mo embedded into Au layer	1.1	300-W Xenon lamp	[14]
$RhCrO_x$/ $SrTiO_3$:Al	0.4	300-W Xenon lamp	[15]
$Rh_{2-y}Cr_yO_3$ loaded Al:$SrTiO_3$	0.11	Xe lamp (wattage not specified)	[16]
TiO_2/CoOOH/$RhCrO_x$ /$SrTiO_3$:Al	0.4	300-W Xenon lamp	[17]
Rh/Cr_2O_3 /CoOOH loaded $SrTiO_3$:Al	0.65	300-W Xenon lamp	[18]
$SrTiO_3$/$Bi_4Ti_3O_{12}$ nanoheterostructural platelet	**0.19**	**300-W Xenon lamp**	**This work**

Supporting information references:

(1) Zhao, Z.; Willard, E. J.; Li, H.; Wu, Z.; Castro, R. H. R.; Osterloh, F. E. Aluminum Enhances Photochemical Charge Separation in Strontium Titanate Nanocrystal Photocatalysts for Overall Water Splitting. *J. Mater. Chem. A* **2018**, *6* (33), 16170–16176. https://doi.org/10.1039/c8ta05885g.

(2) Kuang, Q.; Yang, S. Template Synthesis of Single-Crystal-like Porous $SrTiO_3$ Nanocube Assemblies and Their Enhanced Photocatalytic Hydrogen Evolution. *ACS Appl. Mater. Interfaces* **2013**, *5* (9), 3683–3690. https://doi.org/10.1021/am400254n.

(3) Puangpetch, T.; Sreethawong, T.; Yoshikawa, S.; Chavadej, S. Hydrogen Production from Photocatalytic Water Splitting over Mesoporous-Assembled $SrTiO_3$ Nanocrystal-Based Photocatalysts. *J. Mol. Catal. A Chem.* **2009**, *312* (1–2), 97–106. https://doi.org/10.1016/j.molcata.2009.07.012.

(4) Huang, B. S.; Wey, M. Y. Properties and H_2 Production Ability of Pt Photodeposited on the Anatase Phase Transition of Nitrogen-Doped Titanium Dioxide. *Int. J. Hydrogen Energy* **2011**, *36* (16), 9479–9486. https://doi.org/10.1016/j.ijhydene.2011.05.064.

(5) Wu, Z. L.; Wang, C. H.; Zhao, B.; Dong, J.; Lu, F.; Wang, W. H.; Wang, W. C.; Wu, G. J.; Cui, J. Z.; Cheng, P. A Semi-Conductive Copper-Organic Framework with Two Types of Photocatalytic Activity. *Angew. Chemie - Int. Ed.* **2016**, *55* (16), 4938–4942. https://doi.org/10.1002/anie.201508325.

(6) Zhang, G.; Lan, Z. A.; Lin, L.; Lin, S.; Wang, X. Overall Water Splitting by Pt/g-C_3N_4 Photocatalysts without Using Sacrificial Agents. *Chem. Sci.* **2016**, *7* (5), 3062–3066. https://doi.org/10.1039/c5sc04572j.

(7) Wang, Q.; Hisatomi, T.; Ma, S. S. K.; Li, Y.; Domen, K. Core/Shell Structured La- and Rh-Codoped $SrTiO_3$ as a Hydrogen Evolution Photocatalyst in Z-Scheme Overall Water Splitting under Visible Light Irradiation. *Chem. Mater.* **2014**, *26* (14), 4144–4150. https://doi.org/10.1021/cm5011983.

(8) Makuła, P.; Pacia, M.; Macyk, W. How To Correctly Determine the Band Gap Energy of Modified Semiconductor Photocatalysts Based on UV-Vis Spectra. *J. Phys. Chem. Lett.* **2018**, *9* (23), 6814–6817. https://doi.org/10.1021/acs.jpclett.8b02892.

(9) Lin, X. P.; Huang, F. Q.; Wang, W. D.; Zhang, K. L. A Novel Photocatalyst $BiSbO_4$ for Degradation of Methylene Blue. *Appl. Catal. A Gen.* **2006**, *307* (2), 257–262. https://doi.org/10.1016/j.apcata.2006.03.057.

(10) Mousavi, M.; Habibi-Yangjeh, A.; Abitorabi, M. Fabrication of Novel Magnetically Separable Nanocomposites Using Graphitic Carbon Nitride, Silver Phosphate and Silver Chloride and Their Applications in Photocatalytic Removal of Different Pollutants Using Visible-Light Irradiation. *J. Colloid Interface Sci.* **2016**, *480*, 218–231. https://doi.org/10.1016/j.jcis.2016.07.021.

(11) Cao, T.; Li, Y.; Wang, C.; Zhang, Z.; Zhang, M.; Shao, C.; Liu, Y. $Bi_4Ti_3O_{12}$ Nanosheets/TiO_2 Submicron Fibers Heterostructures: In Situ Fabrication and High Visible Light Photocatalytic Activity. *J. Mater. Chem.* **2011**, *21* (19), 6922–6927. https://doi.org/10.1039/c1jm10343a.

(12) Mulliken, R. S. A New Electroaffinity Scale; Together with Data on Valence States and on Valence Ionization Potentials and Electron Affinities. *J. Chem. Phys.* **1934**, *2* (11), 782–793. https://doi.org/10.1063/1.1749394.

(13) Mulliken, R. S. Electronic Structures of Molecules XI. Electroaffinity, Molecular Orbitals and Dipole Moments. *J. Chem. Phys.* **1935**, *3* (9), 573–585. https://doi.org/10.1063/1.1749731.

(14) Wang, Q.; Hisatomi, T.; Jia, Q.; Tokudome, H.; Zhong, M.; Wang, C.; Pan, Z.; Takata, T.; Nakabayashi, M.; Shibata, N.; Li, Y.; Sharp, I. D.; Kudo, A.; Yamada, T.; Domen, K. Scalable Water

Splitting on Particulate Photocatalyst Sheets with a Solar-to-Hydrogen Energy Conversion Efficiency Exceeding 1%. *Nat. Mater.* **2016**, *15* (6), 611–615. https://doi.org/10.1038/nmat4589.

(15) Goto, Y.; Hisatomi, T.; Wang, Q.; Higashi, T.; Ishikiriyama, K.; Maeda, T.; Sakata, Y.; Okunaka, S.; Tokudome, H.; Katayama, M.; Akiyama, S.; Nishiyama, H.; Inoue, Y.; Takewaki, T.; Setoyama, T.; Minegishi, T.; Takata, T.; Yamada, T.; Domen, K. A Particulate Photocatalyst Water-Splitting Panel for Large-Scale Solar Hydrogen Generation. *Joule* **2018**, *2* (3), 509–520. https://doi.org/10.1016/j.joule.2017.12.009.

(16) Zhao, Z.; Goncalves, R. V.; Barman, S. K.; Willard, E. J.; Byle, E.; Perry, R.; Wu, Z.; Huda, M. N.; Moulé, A. J.; Osterloh, F. E. Electronic Structure Basis for Enhanced Overall Water Splitting Photocatalysis with Aluminum Doped $SrTiO_3$ in Natural Sunlight. *Energy Environ. Sci.* **2019**, *12* (4), 1385–1395. https://doi.org/10.1039/c9ee00310j.

(17) Lyu, H.; Hisatomi, T.; Goto, Y.; Yoshida, M.; Higashi, T.; Katayama, M.; Takata, T.; Minegishi, T.; Nishiyama, H.; Yamada, T.; Sakata, Y.; Asakura, K.; Domen, K. An Al-Doped $SrTiO_3$ Photocatalyst Maintaining Sunlight-Driven Overall Water Splitting Activity for over 1000 h of Constant Illumination. *Chem. Sci.* **2019**, *10* (11), 3196–3201. https://doi.org/10.1039/c8sc05757e.

(18) Takata, T.; Jiang, J.; Sakata, Y.; Nakabayashi, M.; Shibata, N.; Nandal, V.; Seki, K.; Hisatomi, T.; Domen, K. Photocatalytic Water Splitting with a Quantum Efficiency of Almost Unity. *Nature* **2020**, *581* (7809), 411–414. https://doi.org/10.1038/s41586-020-2278-9.